Science Translational Medicine
AAAS

A HIF-Regulated VHL-PTP1B-Src Signaling Axis Identifies a Therapeutic Target in Renal Cell Carcinoma

Natsuko Suwaki, *et al.*

Sci Transl Med **3**, 85ra47 (2011);
DOI: 10.1126/scitranslmed.3002004

Editor's Summary

Detecting Sensitivity to Src Inhibitors

Typically, tumor suppressors are welcome tenants in cells, protecting them from becoming cancerous. But in a twist of fate, 40% of patients with renal cell carcinoma (RCC) regard the presence of a functional tumor suppressor —the von Hippel-Lindau (VHL) protein—as bad news. And for good reason. In contrast to the other 60% of RCC patients whose tumors are driven by the loss of intact VHL, the tumor-suppressor positive cancers are more likely to be resistant to immunotherapy and chemotherapy, and because researchers do not know what drives tumorigenesis, no rational targeted therapies exist. Not content to wait for another twist of fate, Suwaki et al. have delved deeply into these kidney cancers and found that VHL functions as part of an activated signaling pathway that renders the cells sensitive to anticancer agents that target the Src oncoprotein. The presence of VHL and other markers of this pathway can flag those RCC patients who may benefit from drugs that block Src kinase activity.

Enhanced activity of the Src tyrosine kinase has been implicated in cancer development and is the target of the anticancer drug dasatinib. By measuring the extent of phosphorylation of critical proteins in a pair of cell lines with and without functional VHL, the authors saw that Src and its substrates were activated only when VHL was present. And in 215 RCCs, the presence of VHL tended to be associated with highly active Src kinase. Dasatinib inhibited DNA synthesis and cell growth only in cells with VHL, whether they were grown in culture or as xenografts in mice. The authors also replicated the well-known ability of VHL to negatively regulate the hypoxia-sensitive transcription factor HIF, which is activated indirectly by Src. As expected, expression of HIF in VHL-containing cancer cells conferred resistance to dasatinib. An independent analysis of this pathway in tumor samples from an additional 131 patients with RCC confirmed the positive correlation between VHL and Src and its associated pathway proteins. Here, the authors used quantitative phosphoproteomics and immunohistochemical profiling to show the correlation. Because they used automated digital image analysis and an unsupervised hierarchical clustering of the tumors on the basis of the expression of VHL, Src, pFAK and PTP1B, this approach has the potential to be used in the clinic for tumor characterization.

Personalized approaches to cancer treatment require an armamentarium of matched pairs of drugs and validated biomarkers that predict response to therapy. The markers for an activated Src pathway discerned by the authors could in theory be assessed in any solid cancer; in fact, a test in bladder carcinomas showed that, as in RCCs, the Src pathway proteins were activated. If such a test can be applied to many solid cancers, physicians could use it to predict whether a patient is likely to respond to anti-Src agents.

Science Translational Medicine (print ISSN 1946-6234; online ISSN 1946-6242) is published weekly, except the last week in December, by the American Association for the Advancement of Science, 1200 New York Avenue NW, Washington, DC 20005.

CANCER

A HIF-Regulated VHL-PTP1B-Src Signaling Axis Identifies a Therapeutic Target in Renal Cell Carcinoma

Natsuko Suwaki,[1*†] Elsa Vanhecke,[1*‡] Katelyn M. Atkins,[2] Manuela Graf,[1] Katherine Swabey,[1] Paul Huang,[1] Peter Schraml,[3] Holger Moch,[3] Amy Mulick Cassidy,[4] Daniel Brewer,[5] Bissan Al-Lazikani,[6] Paul Workman,[6] Johann De-Bono,[4] Stan B. Kaye,[4] James Larkin,[7] Martin. E. Gore,[7] Charles L. Sawyers,[8] Peter Nelson,[9] Tomasz M. Beer,[10] Hao Geng,[10] Lina Gao,[10] David Z. Qian,[10] Joshi J. Alumkal,[10] Gary Thomas,[2] George V. Thomas[1,10§]

Metastatic renal cell carcinoma (RCC) is a molecularly heterogeneous disease that is intrinsically resistant to chemotherapy and radiotherapy. Although therapies targeted to the molecules vascular endothelial growth factor and mammalian target of rapamycin have shown clinical effectiveness, their effects are variable and short-lived, underscoring the need for improved treatment strategies for RCC. Here, we used quantitative phosphoproteomics and immunohistochemical profiling of 346 RCC specimens and determined that Src kinase signaling is elevated in RCC cells that retain wild-type von Hippel-Lindau (VHL) protein expression. RCC cell lines and xenografts with wild-type VHL exhibited sensitivity to the Src inhibitor dasatinib, in contrast to cell lines that lacked the VHL protein, which were resistant. Forced expression of hypoxia-inducible factor (HIF) in RCC cells with wild-type VHL diminished Src signaling output by repressing transcription of the Src activator protein tyrosine phosphatase 1B (PTP1B), conferring resistance to dasatinib. Our results suggest that a HIF-regulated VHL-PTP1B-Src signaling pathway determines the sensitivity of RCC to Src inhibitors and that stratification of RCC patients with antibody-based profiling may identify patients likely to respond to Src inhibitors in RCC clinical trials.

INTRODUCTION

Renal cell carcinoma (RCC) is the most lethal genitourinary cancer, accounting for about 209,000 new cancer occurrences and 102,000 deaths per year worldwide (*1*). Cure rates in RCC are modest because more than a quarter of patients have metastatic disease at presentation, and patients treated surgically for localized cancers frequently relapse with metastatic disease (*2*, *3*).

RCC is histologically heterogeneous. Although ~75% of RCC are clear cell carcinomas, papillary, chromophobe, sarcomatoid, collecting duct, and medullary carcinomas also occur (*4*). Inactivation of the von Hippel-Lindau (*VHL*) tumor suppressor gene is the most prevalent driver mutation, accounting for ~60% of all RCC tumors and occurring primarily in the clear cell subtype (*5*, *6*). *VHL* loss stabilizes hypoxia-inducible factor–1α (HIF-1α) and HIF-2α, leading to increased expression of HIF-responsive genes, including *VEGF-A*, *PDGF-B*, and *TGF-A* (*6*). HIF-dependent gene expression is further elevated by mammalian target of rapamycin (mTOR), thereby identifying several therapeutic targets in VHL-negative RCC (*7*). Indeed, drugs that target vascular endothelial growth factor (VEGF) and mTOR show clinical activity in patients with metastatic RCC, although these responses are often variable and short-lived (*8*, *9*).

The remaining ~40% of patients with VHL-positive RCCs suffer from a lack of biologically rational treatment options, a result of a paucity of identified molecular drivers. Furthermore, patients with papillary RCC and other non–clear cell RCC are often excluded from clinical trials (*10*, *11*), suggesting that identification of predictive biomarkers that stratify patients for rational treatment strategies is urgently required. Indeed, the ability of the Bcr-Abl inhibitor imatinib to successfully treat chronic myeloid leukemia supports such an approach and has led to the development of targeted therapies for other cancers (*12*–*14*). Targeted therapies are most effective in treating homogenous cancers driven by a single activating oncogene and are much less effective against molecularly heterogeneous cancers such as RCC (*8*). Indeed, quantitative phosphoproteomic studies show that cancer is driven by aberrant networks rather than discrete signaling pathways (*15*, *16*). This observation is exemplified by Src kinase, which, despite its pivotal role in tumor growth, angiogenesis, and metastasis, is rarely mutated in cancer. Rather, Src's signaling output is controlled posttranslationally by the convergent action of the lipid raft–localized inhibitory receptor tyrosine kinase Csk and the activating tyrosine phosphatase PTP1B (protein tyrosine phosphatase 1B) (*17*).

Here, we report a personalized medicine approach for stratifying tumors on the basis of the HIF-regulated VHL-PTP1B-Src signaling axis in patients with VHL-positive RCC that may identify patients likely to respond to Src inhibitors as a co- or monotherapy.

[1]Section of Cell and Molecular Biology, Institute of Cancer Research, Sutton, Surrey SM2 5NG, UK. [2]Vollum Institute, Oregon Health and Science University, Portland, OR 97239, USA. [3]Institute of Surgical Pathology, University Hospital Zurich, Zurich CH-8091, Switzerland. [4]Section of Medicine, Institute of Cancer Research, Sutton, Surrey SM2 5NG, UK. [5]Section of Molecular Carcinogenesis, Institute of Cancer Research, Sutton, Surrey SM2 5NG, UK. [6]Cancer Research UK Center for Therapeutics, Division of Cancer Therapeutics, Institute of Cancer Research, Sutton, Surrey SM2 5NG, UK. [7]Royal Marsden Hospital, London SW3 6JJ, UK. [8]Human Oncology and Pathogenesis Program, Memorial Sloan-Kettering Cancer Center, New York, NY 10065, USA. [9]Divisions of Human Biology and Clinical Research, Fred Hutchinson Cancer Research Center, Seattle, WA 98109, USA. [10]OHSU Knight Cancer Institute, Oregon Health and Science University, Portland, OR 97239, USA.
*These authors contributed equally to this work.
†Present address: Gray Institute for Radiation Oncology and Biology, University of Oxford, Oxford OX3 7DQ, UK.
‡Present address: INSERM U981, Institut de Cancérologie Gustave-Roussy, 94805 Villejuif Cedex, France.
§To whom correspondence should be addressed. E-mail: thomasge@ohsu.edu

RESULTS

Src is expressed in RCC and correlates with VHL expression

To identify cellular signaling networks differentially regulated in RCC subgroups, we performed quantitative phosphoproteomics on SN12C clear cell carcinoma cells, which retain VHL protein expression, and its isogenic subline SN12C-shVHL, which has reduced VHL by short hairpin RNA (shRNA) knockdown (*7*, *18*–*20*). Lysates from parallel cultures of serum-stimulated SN12C and SN12C-shVHL cells were labeled with iTRAQ 8-plex reagent, and phosphotyrosine-containing peptides were subjected to immobilized metal affinity chromatography–tandem mass spectrometry (MS/MS) analysis (*15*). Quantitative phosphorylation profiles were generated for 22 phosphorylation sites, whereas cluster analysis revealed a >50% reduction of pTyr at numerous phosphorylation sites in SN12C-shVHL lysates (Fig. 1A and table S1). Specifically, the proportion of pY^{419} autophosphorylated Src as well as several Src substrates, including annexin II, paxillin, and inositol polyphosphate phosphatase-like 1 (INPPL1), were diminished in SN12C-shVHL lysates. The ability of serum to increase pTyr levels of Src substrates in SN12C cells but not SN12C-shVHL cells suggested that VHL expression is a key determinant of Src kinase activity. Consistent with this possibility, in vitro kinase assays showed that SN12C cells contained about twice as much dasatinib-sensitive Src kinase activity as did SN12C-shVHL cells (Fig. 1B). Together, these data suggest that VHL may regulate Src kinase activity as well as its downstream signaling.

Because both the amount of total Src protein and its enzyme activity are implicated in cancer development (*17*, *21*, *22*), we analyzed a human RCC tissue microarray (TMA) with samples from 215 patients for Src protein expression by immunohistochemistry (Fig. 1C). We found a significant positive association between total Src protein, which correlates with cytoplasmic staining, and active Src, which correlates with membranous staining ($P = 0.0185$, table S2A). RCC samples with strong Src immunostaining came from patients with reduced survival when compared to patients whose samples had weak expression ($P = 0.0367$; Fig. 1D). In addition, multivariate analysis with stage [grouped as organ-confined (pT1, 2) or advanced (pT3, 4)] and Fuhrman grade revealed that strong Src levels independently predicted poorer survival ($P = 0.02$, table S2B). Indeed, there was a tendency for tumors staining negatively for VHL to have weaker Src staining (table S2C).

VHL-WT RCC cells are sensitive to dasatinib

To evaluate whether VHL expression determined sensitivity to Src inhibitors, we treated SN12C and SN12C-shVHL cells as well as ACHN or ACHN-shVHL papillary RCC cells with dasatinib (*7*, *18*–*20*). We found that dasatinib reduced proliferation of VHL-WT SN12C and ACHN cells but not their shVHL counterparts (Fig. 2A). The inhibition of proliferation by dasatinib correlated with an increase in G_1-arrested cells and a corresponding decrease in S-phase cells as determined by propidium iodide (PI) staining (Table 1). Moreover, 5-bromo-2′-deoxyuridine (BrdU) staining showed that dasatinib caused a dose-dependent decrease in DNA synthesis in VHL-WT SN12C and ACHN cells but not in their shVHL counterparts (Fig. 2B). No accumulation of a sub-G_1 population was observed, suggesting that dasatinib is cytostatic in the cell lines tested. Similar results were obtained with VHL-WT RXF-393 and Caki-1 RCC cells compared to VHL-null 786-0 cells (figs. S1 and S2). Correspondingly, ectopic expression of VHL in 786-0 cells conferred increased sensitivity to dasatinib (fig. S2).

Our determination that dasatinib inhibited proliferation of VHL-WT RCC cells prompted us to test whether dasatinib inhibited Src kinase activation and the phosphorylation of Src substrates. Indeed, flow cytometric and immunoblot analyses showed that dasatinib reduced

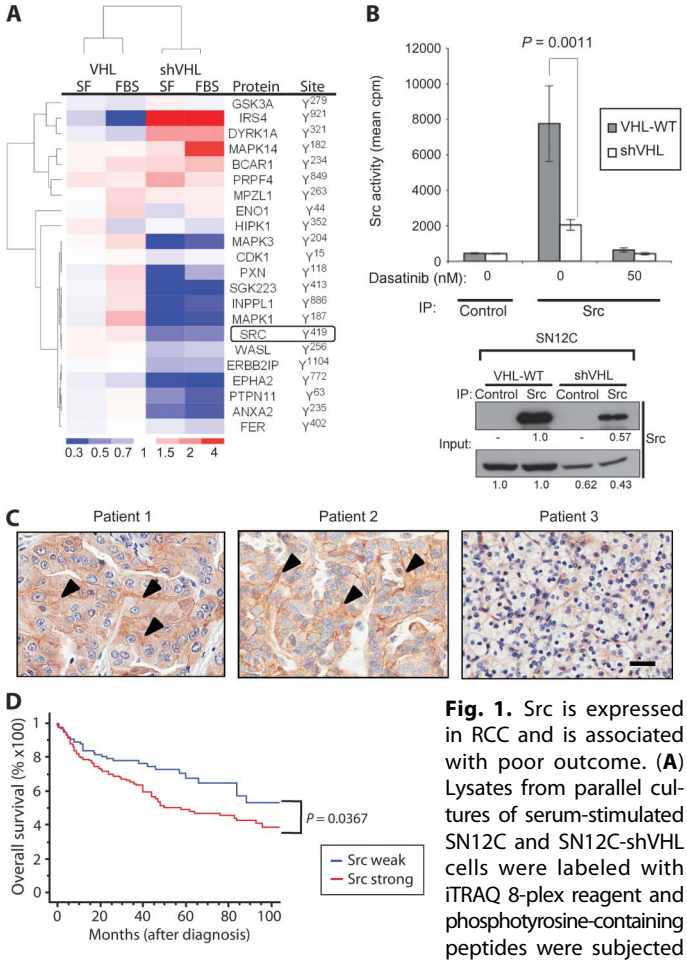

Fig. 1. Src is expressed in RCC and is associated with poor outcome. (**A**) Lysates from parallel cultures of serum-stimulated SN12C and SN12C-shVHL cells were labeled with iTRAQ 8-plex reagent and phosphotyrosine-containing peptides were subjected to immobilized metal affinity chromatography–MS/MS analysis. Quantitative phosphorylation profiles were generated for 22 phosphorylation sites. Mean ratios to SN12C control were log-transformed and partitioned according to similarity of phosphorylation status by unsupervised hierarchical clustering with Cluster 3.0 (*45*) and visualized with TreeView (*46*). Heat map is pseudocolored to indicate direction and magnitude of mean ratios relative to SN12C control cells. SF, serum free; FBS, fetal bovine serum. See also table S1 and Materials and Methods. (**B**) Src was immunoprecipitated from SN12C and SN12C shVHL cells, and Src kinase activity was measured in the absence or presence of 50 nM dasatinib as described in Materials and Methods. Data are presented as the mean cpm (counts per minute) ± SD from three independent experiments assayed in duplicate. (Lower panel) Corresponding Western blot showing control (no primary antibody) or Src immunoprecipitates and relative Src expression in SN12C and SN12C-shVHL cells. The amount of Src was quantified with ImageJ and presented as mean cpm. (**C**) Immunohistochemistry for Src from samples from three representative RCC patients with strong (left and middle panels) or weak expression (right panel). Arrowheads indicate membranous localization. Scale bar, 20 μm. (**D**) Kaplan-Meier survival analysis of clear cell RCC patients with tumors expressing weak or strong Src immunohistochemical staining ($n = 117$, $P = 0.0367$).

pY^{419} Src levels irrespective of VHL status (Fig. 2C). In agreement with the in vitro kinase assay (Fig. 1B), Western blot analysis showed that pY^{419} Src levels were higher in VHL-WT SN12C or ACHN cells compared to their shVHL counterparts. Dasatinib also caused total Src protein levels to increase regardless of VHL status (Fig. 2C and fig. S2). This dasatinib-induced increase in total Src protein has been observed in other tumor types as well as with other classes of Src inhibitors and is consistent with the increased stability of dephosphorylated Src in vivo (*23*–*26*). In addition to inhibiting pY^{419} Src, dasatinib inhibited phosphorylation of the Src substrate FAK in VHL-WT cells (Fig. 2C). Surprisingly, pY$^{576/577}$ FAK was undetectable in VHL knockdown cells despite the presence of total FAK protein. These results suggest that dasatinib may selectively inhibit proliferation of VHL-WT cells compared to their VHL-null or VHL-low counterparts by repressing Src's signaling output.

To evaluate the effect of dasatinib on tumor growth in vivo, we implanted SN12C and SN12C-shVHL cells subcutaneously into the flanks of nude mice. Daily treatment with dasatinib significantly reduced the growth of VHL-WT SN12C cells but had no effect on SN12C-shVHL cells, recapitulating our in vitro findings (compare Fig. 2, A and D). Dasatinib had no statistically significant effect on apoptosis in the xenograft tumors. Notably, administration of dasatinib resulted in a statistically significant reduction of Ki-67–positive proliferating SN12C cells but not SN12C-shVHL cells (Fig. 2E). Together, these results demonstrate that VHL-WT RCC cells are more sensitive than shVHL cells to dasatinib in xenograft tumors as well as in vitro and that this sensitivity is mediated through a blockade on proliferation.

Next, we asked whether the dasatinib-induced growth inhibitory effects on VHL-WT RCC cells were due to Src inhibition. Indeed, SN12C cells knocked down for Src (SN12C-shSrc) were resistant to dasatinib treatment (Fig. 3A). By contrast, rescue of SN12C-shSrc cells by expression of chicken Src, which is resistant to the human-specific shRNA (*27*), restored dasatinib sensitivity. Moreover, stable expression of a dasatinib-resistant Src encoding a T388I gatekeeper mutation, which prevents access of adenosine 5′-triphosphate (ATP)–competitive inhibitors to the ATP-binding pocket in Src, thereby protecting pY^{419} autophosphorylation, conferred resistance of SN12C cells to dasatinib (Fig. 3B) (*27*, *28*). Similarly, expression of v-Src, which naturally expresses the T→I gatekeeper mutation (*29*), rendered VHL-WT SN12C and ACHN cells resistant to dasatinib (Fig. 3C and fig. S3). Accordingly, SN12C–v-Src xenograft tumors grown in severe combined

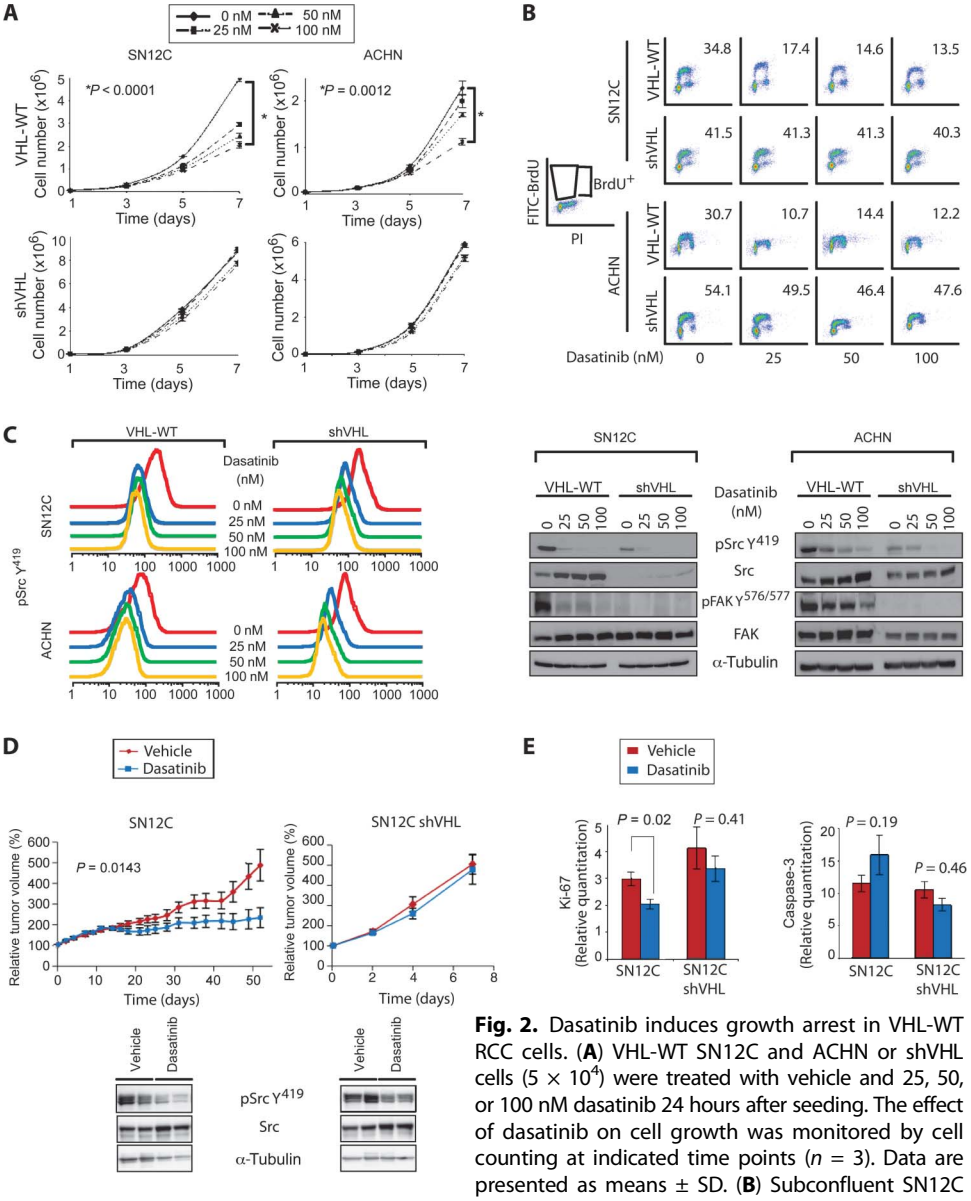

Fig. 2. Dasatinib induces growth arrest in VHL-WT RCC cells. (**A**) VHL-WT SN12C and ACHN or shVHL cells (5×10^4) were treated with vehicle and 25, 50, or 100 nM dasatinib 24 hours after seeding. The effect of dasatinib on cell growth was monitored by cell counting at indicated time points (n = 3). Data are presented as means ± SD. (**B**) Subconfluent SN12C and ACHN VHL-WT or shVHL cells were treated with the indicated doses of dasatinib for 48 hours and labeled with 10 μM BrdU for 30 min before harvesting. Cells were dual-stained with fluorescein isothiocyanate (FITC)–BrdU antibody and PI and analyzed by flow cytometry. (**C**) Subconfluent SN12C and ACHN VHL-WT or shVHL cells were treated with vehicle and 25, 50, or 100 nM dasatinib. Inhibitory effect of dasatinib on Src kinase activity was assessed by flow cytometry with anti-pY^{419} Src (left panel). Levels of total and phospho-specific forms of Src and FAK were determined by immunoblotting (right panel). α-Tubulin was used as the loading control. (**D**) Nude mice bearing SN12C and SN12C shVHL xenografts were treated daily with vehicle or dasatinib (10 mg/kg) by oral gavage. Fold increase in tumor volume is plotted against days following tumor injection. Xenografts were analyzed by immunoblot for levels of pY^{419} Src and total Src. α-Tubulin was used as the loading control. Data are presented as means ± SEM of six mice in each group. (**E**) Xenograft tumors from (D) were analyzed for cell proliferation and apoptosis by immunohistochemistry against Ki-67 and cleaved caspase-3, respectively, and subjected to quantitative image analysis. Data are presented as means ± SEM (n = 11 to 21).

Table 1. Cell cycle analysis of shVHL lines. VHL-WT or shVHL SN12C and ACHN cell lines were treated with the indicated concentration of dasatinib, and cell cycle profiles were examined by flow cytometry. Cell population (%) in each cell cycle phase was quantified.

	Dasatinib (nM)			
	0	25	50	100
SN12C				
VHL-WT				
G_1	52.4	59.5	63.6	70.0
S	30.9	23.9	22.8	16.3
G_2-M	15.4	15.0	11.7	11.7
shVHL				
G_1	45.0	45.2	45.4	46.1
S	35.6	36.9	38.5	35.3
G_2-M	19.1	17.5	15.7	18.5
ACHN				
VHL-WT				
G_1	54.7	59.7	62.1	64.5
S	26.5	25.8	17.6	15.7
G_2-M	16.8	12.6	16.0	14.9
shVHL				
G_1	51.4	50.2	47.6	46.1
S	33.0	37.4	36.7	40.8
G_2-M	13.9	9.8	14.2	10.9

immunodeficient (SCID) mice were resistant to dasatinib, whereas parental SN12C tumors remained dasatinib-sensitive (Fig. 3D).

Several controls supported our findings that dasatinib suppressed proliferation in VHL-WT cells by inhibiting Src. First, SN12C cells expressing the BCR-ABL T315I gatekeeper mutant were sensitive to dasatinib, suggesting the dasatinib resistance mediated by Src T388I or v-Src was specific (fig. S4). Second, treatment with imatinib, which inhibits ABL, PDGFR (platelet-derived growth factor receptor), and c-KIT but not Src, had no effect on the proliferation of SN12C or SN12C-shVHL cells (fig. S5A). Finally, saracatinib, a structurally unrelated Src inhibitor (*30*), repressed proliferation of control SN12C cells but not shVHL cells (fig. S5B).

Constitutively stabilized HIF confers resistance to dasatinib in VHL-WT cells

Because the E3 ligase activity of VHL negatively regulates HIF, we asked whether expression of constitutively stable HIF would phenocopy VHL loss by conferring resistance to dasatinib in VHL-WT RCC cells. Indeed, SN12C and ACHN cells expressing constitutively stable HIF-1α–P564A or HIF-2α–P405A,P531A mutants (*31*) contained reduced levels of Src mRNA and were resistant to the dasatinib-mediated G_1 arrest observed in parental SN12C and ACHN cells (Fig. 4, A to C, fig. S6, and Table 2). Correspondingly, constitutively stable HIF-1α and HIF-2α inhibited Src signaling output in VHL-WT RCC cells as determined by immunoblot of pY^{419} Src and phosphorylated Src substrates, including $pY^{576/577}$ FAK, pY^{703}STAT3, and pY^{204}ERK (Fig. 4D).

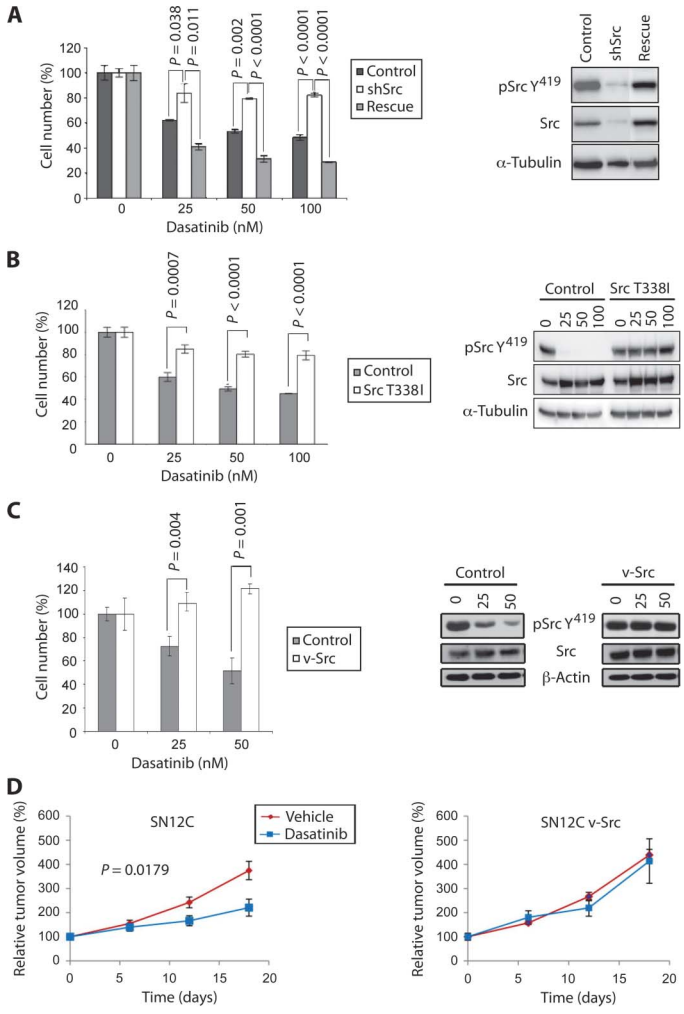

Fig. 3. Src is the relevant target of dasatinib in RCC. (**A**) SN12C, SN12C-shSrc, or SN12-shSrc cells expressing shRNA-resistant Src (Rescue) were treated with vehicle and 25, 50, or 100 nM dasatinib for 96 hours and then cell growth was analyzed by cell count. Data are presented as means ± SD (n = 3). Src expression or knockdown was verified by immunoblot with antibodies against total and pY^{419} Src. α-Tubulin was used as the loading control. (**B** and **C**) SN12C cells (Control) or SN12C cells stably expressing (B) dasatinib-resistant Src (Src T338I) or (C) v-Src were treated with vehicle alone or with 25 or 50 nM dasatinib for 96 hours and then cell growth was analyzed by cell count. Data are presented as means ± SD (n = 3). The levels of total Src and pY^{419} Src were assessed by immunoblot. α-Tubulin and β-actin were used as loading controls. (**D**) SCID mice bearing SN12C and SN12C v-Src xenografts were treated daily with vehicle or dasatinib (10 mg/kg) by oral gavage. Percent (%) increase in tumor volume is plotted against days after tumor injection. Data are presented as means ± SEM (n = 24).

Conversely, ectopic expression of VHL in VHL-null 786-0 RCC cells resulted in an increase in both total and pY^{419} Src, as well as the phosphorylation and activation of its downstream targets when compared to the parental cells (figs. S2 and S7). Together, these results suggest that HIF represses VHL-mediated Src signaling output.

The ability of constitutively stable HIF mutants to promote dasatinib resistance and repress Src signaling output suggested that HIF may repress an activator of Src activity. Consistent with this possibility, expression

of PTP1B protein and mRNA, which activates Src by dephosphorylation of Y^{530}, was consistently lower in shVHL or RCC cells that ectopically express constitutively stable HIF (Fig. 4, D and E). Correspondingly, PTP1B protein was decreased in VHL-null 786-0 cells compared to VHL-restored 786-0–VHL cells (fig. S7). Biochemical analysis of Src signaling output suggested that PTP1B knockdown phenocopied

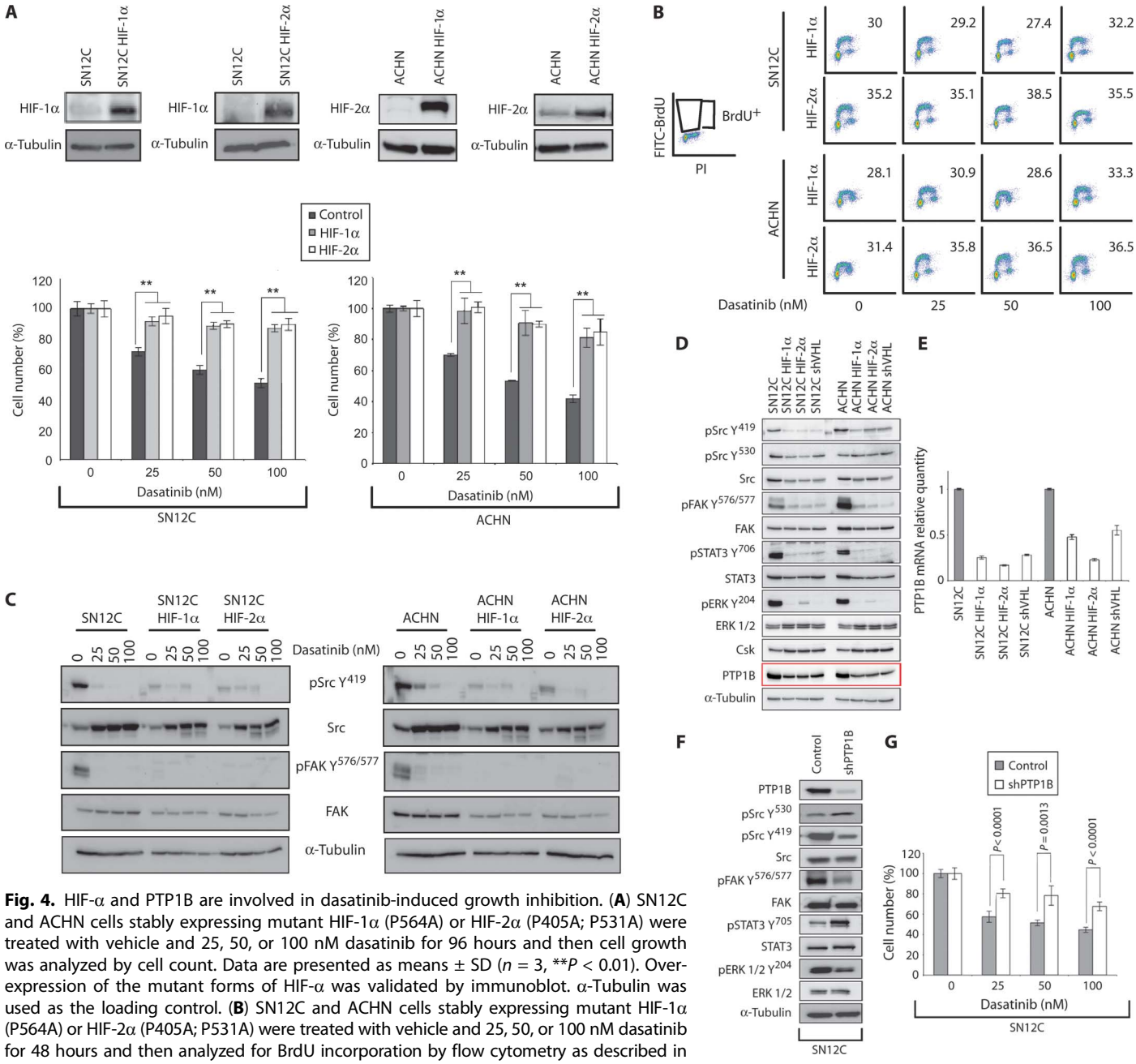

Fig. 4. HIF-α and PTP1B are involved in dasatinib-induced growth inhibition. (**A**) SN12C and ACHN cells stably expressing mutant HIF-1α (P564A) or HIF-2α (P405A; P531A) were treated with vehicle and 25, 50, or 100 nM dasatinib for 96 hours and then cell growth was analyzed by cell count. Data are presented as means ± SD ($n = 3$, $^{**}P < 0.01$). Overexpression of the mutant forms of HIF-α was validated by immunoblot. α-Tubulin was used as the loading control. (**B**) SN12C and ACHN cells stably expressing mutant HIF-1α (P564A) or HIF-2α (P405A; P531A) were treated with vehicle and 25, 50, or 100 nM dasatinib for 48 hours and then analyzed for BrdU incorporation by flow cytometry as described in Materials and Methods. (**C**) SN12C and ACHN cells stably expressing constitutively stable HIF-1α P564A (SN12C HIF-1α) or HIF-2α P405A; P531A (SN12C HIF-2α) were treated with vehicle alone or with 25, 50, or 100 nM dasatinib for 18 hours. Levels of total Src and FAK, as well as pSrc Y^{419} and pFAK $Y^{576/577}$ were determined by immunoblot. α-Tubulin was used as the loading control. (**D**) Lysates from the SN12C and ACHN mutant HIF-α–overexpressing lines, shVHL cells, and the parental cell lines were examined for expression of total and/or phosphospecific forms of Src, FAK, ERK1/2 (extracellular signal–regulated kinase 1/2), STAT3, Csk, and PTP1B by immunoblot. α-Tubulin was used as the loading control. (**E**) The levels of PTP1B mRNA were measured by real-time polymerase chain reaction (PCR) in SN12C and ACHN HIF-α–overexpressing and shVHL cell lines. Levels of PTP1B mRNA in the parental cell lines were normalized to 1. Data are presented as means ± SD ($n = 3$). (**F**) SN12C cells expressing an shRNA targeting PTP1B (shPTP1B) were analyzed by immunoblot for expression levels of total and/or phospho-specific forms of PTP1B, Src, FAK, STAT3, ERK1/2, and α-tubulin. (**G**) SN12C or shPTP1B cells were treated with vehicle and 25, 50, or 100 nM dasatinib, and cell growth was assessed by cell count. Data are presented as means ± SD ($n = 3$).

Table 2. Cell cycle analyses of HIF-α mutant cell lines. Cell cycle profiles of SN12C and ACHN cells expressing constitutively stable HIF-1α–P564A (HIF-1α) or HIF-2α–P405A, P853A (HIF-2α) mutants were analyzed by flow cytometry 48 hours after treatment with dasatinib. Cell population (%) in each cell cycle phase was quantified.

	Dasatinib (nM)			
	0	25	50	100
SN12C				
HIF-1α				
G_1	58.3	60.1	59.2	60.4
S	26.7	25.1	27.6	26.5
G_2-M	13.3	13.3	11.4	11.1
HIF-2α				
G_1	56.4	54.8	55.7	49.7
S	20.9	23.6	21.4	27.8
G_2-M	21.5	20.6	22.1	21.3
ACHN				
HIF-1α				
G_1	57.3	59.2	56.4	60.1
S	21.6	21.6	25.1	17.6
G_2-M	17.7	17.1	16.0	22.0
HIF-2α				
G_1	59.4	53.9	51.9	55.3
S	20.8	27.7	27.0	24.2
G_2-M	17.5	16.1	19.3	17.7

expression of constitutively stable HIF in VHL-WT cells. SN12C-shPTP1B cells contained reduced pY^{419} Src and the levels of phosphorylated Src substrates, including $pY^{576/577}$FAK, and pY^{204}ERK (Fig. 4F), and were relatively resistant to dasatinib-mediated growth inhibition (Fig. 4G). Only pY^{703}STAT3 was unaffected by PTP1B knockdown, which may result from a PTP1B-specific effect on STAT3 (signal transducer and activator of transcription 3) and its regulator, JAK (Janus kinase) (*32*). As a control, SN12C cells were exposed to hypoxia in vitro or in xenograft tumors. We found that HIF was stabilized but PTP1B was unaffected, suggesting that HIF-regulated PTP1B expression may be different under hypoxic conditions (fig. S8).

Consistent with the reduced activation of Src, PTP1B knockdown cells were less sensitive to dasatinib than control cells (Fig. 4G and fig. S9). By contrast, overexpression of the Src regulator Csk in SN12C cells had no effect on dasatinib sensitivity or Src signaling output (fig. S10), which is consistent with work by others that Csk phosphorylation of Src pY^{530} is complex (*33*–*37*) (see Discussion). Together, these results suggest that sensitivity to dasatinib correlates with the inhibition of Src's signaling output.

In addition to repressed levels of PTP1B protein, RCC cells with VHL knockdown or expression of constitutively stable HIF had reduced PTP1B mRNA (Fig. 4E), suggesting that HIF may repress *PTP1B* transcription. In support of this finding, chromatin immunoprecipitation (ChIP) revealed that HIF is enriched at a putative hypoxia response element in the PTP1B promoter in ACHN cells expressing constitutively stable HIF-1α–P564A but not in parental ACHN cells (fig. S11). This result suggests that HIF-mediated transcriptional regulation of the *PTP1B* gene contributes to the repression of Src signaling output in VHL-null RCC cells.

Interaction of VHL, HIF, PTP1B, and Src in RCC patients

Our identification of a HIF-regulated VHL-PTP1B-Src signaling axis in RCC cell lines provided us with additional markers to interrogate the presence of this pathway in RCC patients. We constructed a TMA from a second cohort of 131 patients with RCC and performed immunohistochemistry for VHL, HIF-2α, which is the primary driver in VHL-null RCC (*38*), Src, and PTP1B. As controls, we analyzed the HIF transcriptional target CA-IX, as well as the Src substrate pFAK. Quantification was performed with automated digital image analysis algorithms to rigorously and systematically measure staining intensity (Fig. 5A). An unsupervised hierarchical clustering of the tumors on the basis of the expression of VHL, Src, pFAK, and PTP1B was used to generate a heat map (fig. S12). VHL, Src, PTP1B, and pFAK showed the most similar expression patterns, although pFAK expression was generally lower than the other markers.

In agreement with the initial RCC clinical data set (table S2A), a Spearman rank correlation test of the second RCC clinical data set again revealed a positive correlation between VHL and Src ($r = 0.409$; $P < 0.001$; Fig. 5B). Using these more stringent analyses, only 8% (1 of 12) of VHL-negative tumors had strong Src expression, whereas 58% (69 of 119) of VHL strong tumors had strong Src expression, suggesting a correlative relationship between VHL and Src ($P = 0.0018$; Fig. 5C and table S3). Conversely, the relationship between VHL and HIF-2α revealed a significant negative correlation ($r = -0.132$; $P = 0.036$). In agreement with our in vitro findings, PTP1B positively correlated with VHL ($r = 0.293$; $P < 0.001$) but negatively correlated with HIF-2α ($r = -0.212$; $P = 0.001$), suggesting that patient tumors with VHL loss or HIF-2α overexpression may have reduced PTP1B expression. Controls showed positive correlations between HIF-2α and CA-IX and between Src and pFAK as expected (Fig. 5B). A multiple linear regression showed VHL ($P < 0.0001$) and PTP1B ($P < 0.0001$) to be predictors of Src expression. Additionally, VHL ($P < 0.0001$) and HIF-2α ($P = 0.0021$) were independent predictors of PTP1B levels (Table 3). Next, we extracted the data points and organized them into a scatter plot representing patient subgroups defined by VHL and Src expression (Fig. 5D). Indeed, 28.6% of the patients were VHL strong/Src strong, representing the potential candidates for a prospective Phase II clinical trial with dasatinib (table S3).

Next, we tested whether this RCC immunohistochemistry profile could be applied to other cancers to predict sensitivity to dasatinib. Using a clinical data set of transitional cell carcinomas of the bladder, we found the same correlations among VHL, Src, HIF-2α, and PTP1B (fig. S13). Together, these findings suggest that the immunophenotype of the VHL-PTP1B-Src signaling axis comprises a signature that not only defines a biologically distinct subgroup of RCC that may benefit from dasatinib or similar Src inhibitors but also points to a wider clinical applicability for these predictive markers in identifying sensitivity to Src inhibitors.

We then explored the cooperating events involved in mediating sensitivity to dasatinib by applying a systems-based approach to map the potential protein-protein interactions, transcriptional information, and the signaling networks they affect by using the ROCK-BCFG database (*39*). We seeded the interaction network searches with targets

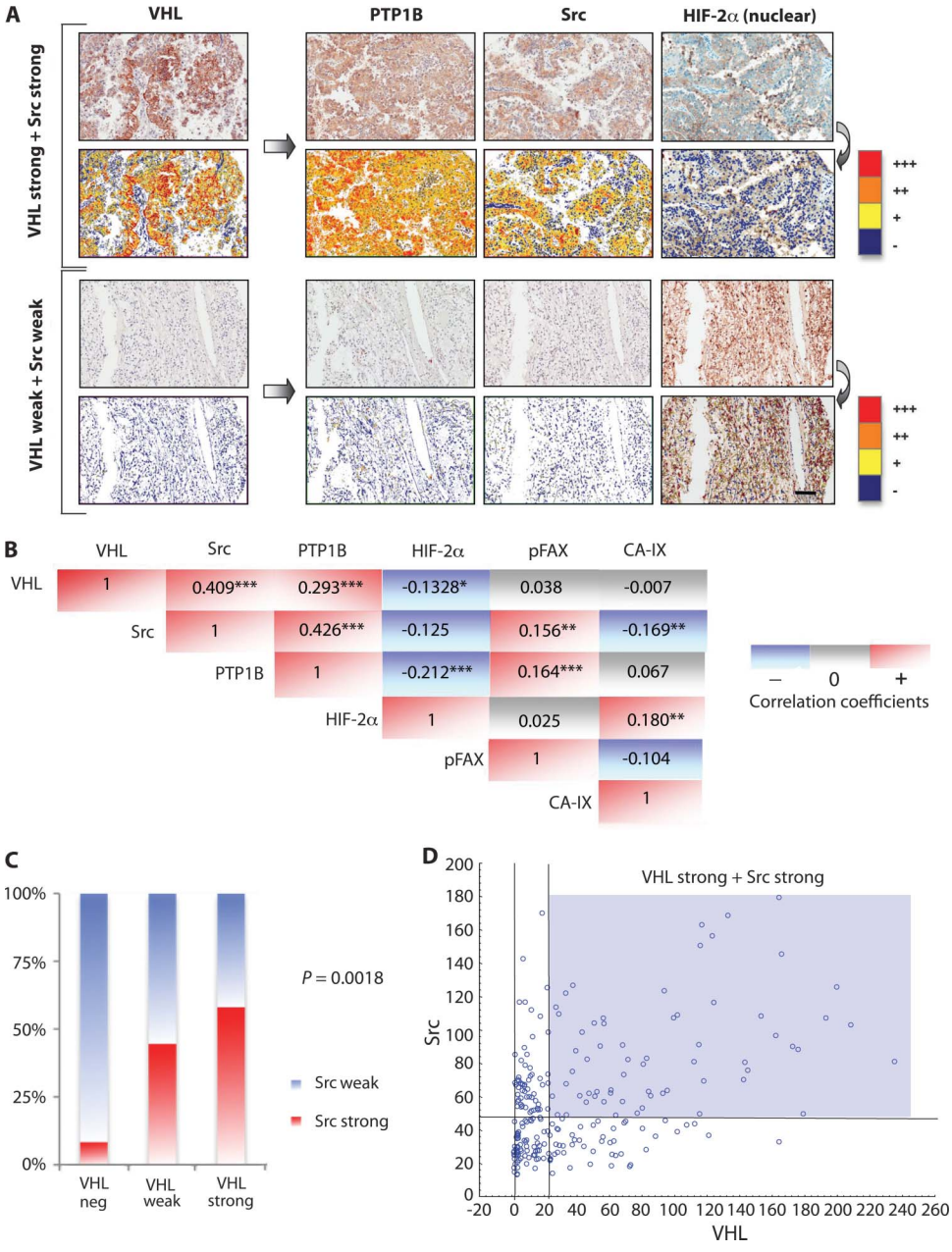

Fig. 5. VHL, HIF-α, Src, and PTP1B levels are related in RCC patients. (**A**) Quantitative assessment of VHL, PTP1B, Src, and HIF-2α expression by immunostaining of RCC TMA. Representative staining images from a patient with strong VHL protein expression (top panel) and from a patient with weak VHL expression (bottom panel) are shown. Corresponding markup images of the color deconvolution algorithm with intensity ranges are shown (red = strong, orange = moderate, yellow = weak, blue = negative immunoreactivity). For HIF-2α, the nuclear immunostaining algorithm was applied. Scale bar, 50 μm. (**B**) Spearman Rho correlation coefficients among the biomarkers. Red indicates positive correlation and blue indicates negative correlation. *P* values for these correlations are represented as follows: **P* < 0.05; ***P* < 0.001; ****P* < 0.0001 (*n* = 131). (**C**) Comparison between Src and VHL protein expression in the samples of the RCC tissue microarray (TMA). (**D**) Scatter plot of the VHL and Src scores generated from automated image analysis intensity algorithm. The vertical lines represent fifth percentile and median VHL scores, corresponding to thresholds for negative and weak expression, respectively. The horizontal line represents the median for the Src score, where levels below are considered weak expression and levels above are considered strong expression. The upper right (shaded) quadrant depicts the molecular phenotype of tumors with both strong VHL and strong Src expression.

identified in our experiments and defined a protein interaction network containing 82 nodes that suggest an underlying signaling network involving Src, PTP1B, CA-IX, FAK, and VHL together with the transcriptional regulators HIF-1α, HIF-2α, and Sp1 (fig. S14).

DISCUSSION

Although targeted therapies have been successful in treating cancers driven by the activation of a single oncogene, these drugs are much less effective in molecularly heterogeneous cancers driven by a multitude of dysregulated signaling networks (*16*). Successful treatment therefore requires a personalized medicine approach based on robust predictive biomarkers that can stratify patients toward appropriate targeted therapies. Here, we used a quantitative phosphoproteomic screen to identify Src as a potential pharmacologic target in metastatic RCC. Immunohistochemistry of 346 human RCC tumors identified a positive correlation between Src and VHL expression, whereas treatment of VHL-WT xenografts with dasatinib blocked tumor growth in vivo. Conversely, forced expression of HIF, which phenocopied *VHL* loss, diminished Src's signaling output by down-regulation of PTP1B, thereby conferring resistance to dasatinib. HIF binds the *PTP1B* promoter and reduces PTP1B expression, suggesting that HIF controls Src signaling output by regulating *PTP1B* transcription. Our data suggest that stratifying RCC patients by profiling for expression of VHL and Src, as well as downstream effector molecules may identify patients likely to respond to Src inhibitors in future RCC clinical trials.

Despite playing a central role in multiple tumorigenic signaling networks, Src itself is rarely mutated in cancers (*17*). Our data suggest that one mechanism by which tumor cells amplify Src kinase activity is by using gene-autonomous drivers such as PTP1B to dephosphorylate the kinase autoinhibitory domain. The ability of PTP1B knockdown to confer resistance to dasatinib (Fig. 4G and fig. S9) suggests that PTP1B may augment Src signaling in RCC cells by channeling inputs from upstream oncogenes, including Ras (*40*). Unlike PTP1B knockdown,

Table 3. Multiple linear regression. Coefficient estimates for two predefined models PTP1B and Src. All variables have been log-transformed. CI, confidence interval.

Outcome and covariates	Estimated coefficient	95% CI	*P*
Src			
VHL	0.146	0.096 to 0.196	2.55×10^{-8}
PTP1B	0.257	0.155 to 0.359	1.20×10^{-6}
Intercept	2.382	1.987 to 2.778	$<2 \times 10^{-16}$
PTP1B			
VHL	0.164	0.104 to 0.225	2.11×10^{-7}
HIF-2α	−0.228	−0.373 to −0.084	0.00211
Intercept	4.298	3.796 to 4.800	$<2 \times 10^{-16}$

overexpression of Csk did not alter Src pY^{419} status (fig. S10), suggesting that the regulation of Src activation by Csk is complex. Our findings are consistent with reports that Csk phosphorylation of Src Y^{530} requires interaction of Csk with Csk-binding protein (Cbp) in lipid rafts (*33*–*37*), suggesting that analysis of Src pY^{419} or pY^{530} levels by immunoblot is insufficient to detect minute or compartment-specific changes in Src activation. Our finding that hypoxia-induced stabilization of HIF failed to affect PTP1B expression is in agreement with the HIF-dependent but hypoxia-independent regulation of Ror2 (fig. S8) (*41*), and is consistent with the model that HIF-mediated inhibition of PTP1B requires that HIF be constitutively stabilized by VHL loss and not by fluctuating O_2 levels present in VHL-WT tumors (*42*). Finally, although our studies cannot exclude the possibility that dasatinib may mediate its effects by inhibiting additional Src family kinases (SFKs), they highlight the therapeutic utility of a pan-SFK inhibitor such as dasatinib.

Successful implementation of targeted therapies in molecularly heterogeneous cancers requires robust predictive biomarkers. The development of epidermal growth factor receptor (EGFR) mutation analysis for stratification of patients with non–small cell lung cancer to EGFR inhibitors supports the feasibility of this approach (*43*). Therefore, our initial examination of VHL and Src on routinely processed human RCC samples assessed the clinical significance of Src expression. Indeed, RCC patient samples with strong Src expression had a statistically significant reduced overall survival when compared to those with weak expression. This analysis also suggested a positive correlation between VHL and Src with a semiquantitative scoring protocol that was biased toward sensitivity relative to specificity. We then more rigorously interrogated the VHL-Src relationship with enhanced specificity by analyzing VHL, Src, as well as their downstream effector molecules in a second cohort of human RCC tumors. This analysis used unbiased digital image analysis algorithms to objectively quantify staining intensities and to determine correlations between these molecules. The VHL-Src relationship was one of the strongest correlations found. In addition, the relationships among VHL, Src, HIF-2α, PTP1B, pFAK, and CA-IX were recapitulated in patient tumors, consistent with our in vitro results. The presence of these associations in clinical samples reveals the strength of the molecular networks identified and supports the testing of these markers in future clinical trials.

Inactivation of the *VHL* tumor suppressor gene is the most prevalent driver mutation in RCC, accounting for ~60% of all tumors (*5*, *6*). Thus, even though ~40% of RCC patients have VHL-positive cancer, they are treated as if they have VHL-negative cancers. Unfortunately, the absence of biomarker-driven treatment protocols in RCC, together with the fact that VHL-positive patients are excluded from many registration trials, precludes meaningful understanding of the mechanisms of response or resistance. Thus, the singular approach targeting VEGF or mTOR, which is currently used to treat metastatic RCC, underscores the need for alternative treatment strategies for VHL-positive metastatic RCC. Our findings suggest that Src inhibition may represent a rational treatment option in renal cancers that retain VHL protein expression. Additionally, analyzing functional readouts of VHL and Src activity by means of HIF, CA-IX, and pFAK expression could enhance specificity because functional VHL would confer low HIF and CA-IX expression, whereas elevated Src signaling output would correlate with increased pFAK levels. Although the ideal treatment subgroup would include those tumors that are VHL strong, Src strong, pFAK strong, HIF weak, and CA-IX weak, the most effective biomarker combination can only be determined from future clinical studies in which outcomes after Src inhibitor treatment are known. Because Src inhibitors such as dasatinib and saracatinib already have been clinically tested, our data suggest that analysis of these potential biomarkers can occur rapidly in a Phase II clinical trial in patients with metastatic RCC.

Collectively, our results suggest that a fundamental change in RCC treatment may be warranted. Specifically, patients should be selected initially on the basis of a molecular phenotype. The simplicity of our approach lies in two elements: use of an immunohistochemical-based assay on routinely processed clinical samples and the targeting of *src*, a well-characterized oncogene for which there already exist clinically active drugs. The key challenges ahead are assessing intratumor heterogeneity and standardization of methods across diagnostic laboratories. In summary, stratifying RCC patients on the basis of the presence of an active VHL-PTP1B-Src signaling axis in the tumor will identify a subgroup likely to respond to Src inhibitors.

MATERIALS AND METHODS

Sample preparation, peptide immunoprecipitation, and MS analysis

SN12C and SN12C-shVHL cells were maintained in Dulbecco's modified Eagle's medium (DMEM) supplemented with 10% fetal bovine serum (FBS). Cells (40 to 50% confluence per 10-cm plate) were seeded for 24 hours, washed twice with phosphate-buffered saline (PBS), and then incubated for 24 hours in serum-free media. Cells were stimulated with 10% serum for 10 min and harvested in 900-μl dish/8 M urea. Unstimulated cells were used as controls. Cells were lysed in 8 M urea and subjected to reduction, alkylation, and trypsin digestion as previously described (*15*). Peptides were desalted on a C18 Sep-Pak Plus cartridge (Waters), eluted with 25% acetonitrile, and lyophilized to dryness. Lyophilized peptides were subjected to labeling with the iTRAQ 8-plex reagent (Applied Biosystems). Peptide immunoprecipitation was performed as described (*15*). Briefly, 30 μg of protein G Plus-agarose beads (Sigma) was incubated with 12 μg of each of the antiphosphotyrosine antibodies [$pTyr^{100}$ (Cell Signaling Technology), PT66 (Perkin Elmer), and 4G10 (Millipore)] in 200 μl of immunoprecipitation buffer (100 mM tris, 100 mM NaCl, 1% NP-40, pH 7.4) for 8 hours at 4°C. Beads were

washed with rinse buffer (100 mM tris, 100 mM NaCl, pH 7.4), and retained peptides were eluted from antibody with 70 μl of elution buffer (100 mM glycine, pH 2.5) for 1 hour at room temperature. Immobilized metal affinity chromatography was performed to enrich for phosphorylated peptides, and peptides retained on the column were eluted with 250 mM sodium phosphate (pH 8.0) and analyzed by electrospray ionization liquid chromatography–MS/MS on a QqTof (QSTAR Elite, Applied Biosystems) as described (*15*).

Phosphopeptide sequencing, quantification, and analysis

MS/MS spectra were extracted, searched, and quantified with Protein Pilot (Applied Biosystems). Phosphorylation sites and peptide sequence assignments were validated by manual confirmation of raw MS/MS data. Peak areas of iTRAQ marker ions [mass/charge ratio (*m/z*) 113, 114, 115, 116, 117, 118, 119, and 121] were normalized with values from the iTRAQ marker ion peak areas of nonphosphorylated peptides in supernatant of the immunoprecipitation. Each condition was normalized against the 113 channels to obtain fold changes across all eight conditions. Table S1 represents the mean and SD of two biological replicate experiments.

Tissue microarrays

Two separate RCC patient clinical databases were used to construct the TMAs described in our experiment. The first TMA comprised 215 clear cell RCCs collected from nephrectomies performed at the University Hospital of Zurich. All RCC samples were histologically reviewed by one pathologist (H.M.). This study was approved by the local commission of ethics. Tumor-specific survival data were obtained by reviewing the hospital records and by the cancer registry of the Canton of Zurich. The second RCC TMA consisted of 131 nephrectomies performed for kidney cancer at the Royal Marsden Hospital, London. This study protocol was approved by the hospital ethics review board. All tumors arrayed from this second data set were histologically reviewed by one pathologist (G.V.T.).

Immunohistochemistry

The first TMA was stained with the *ultra*View Universal DAB Detection Kit (Ventana). A clear cell RCC tumor with strong membranous Src positivity was used as positive control. Negative controls were identical array sections stained in the absence of the primary antibody. Immunohistochemistry can yield false positivity at the margin or edges of tissue (that is, edge effect), and this needs to be considered when scoring TMA cores. Therefore, to minimize false positivity, we used a conservative 5% cutoff; that is, any tumors with <5% cytoplasmic and/or membranous staining were considered negative, and any tumors with >5% cytoplasmic and/or membranous staining were considered positive. Next, positive Src expression was analyzed subjectively based on antibody staining intensity as having either weak or strong cytoplasmic and/or membranous immunoreactivity by an experienced pathologist (H.M.). VHL immunostaining was similarly scored (*44*).

The second TMA was processed with EnVision Kits (Dako), SuperSensitive IHC Detection Systems (BioGenex), or Vectastain ABC Kit (Vector Labs) according to the manufacturer's instruction. Negative control slides were used in every run (incubated in Dako Universal Negative Control Mouse/Rabbit). Diaminobenzidine tetrahydrochloride (DAB) was used as the enzyme substrate for visualization and counterstained with hematoxylin.

Image acquisition, management, and automated analysis

The Aperio ScanScope CS slide scanner (Aperio Technologies) was used to capture whole-slide digital images with a 20× objective. Slides were de-arrayed to visualize individual cores with the TMA Lab (Aperio). A color deconvolution algorithm (Aperio) was used to develop a quantitative scoring model for measuring cytoplasmic immunoreactivity in TMAs consecutively stained with VHL, Src, CA-IX, PTP1B, and pFAK. A nuclear algorithm was used to quantify HIF-2α and Ki-67 nuclear positivity. The algorithm was calibrated to individual staining patterns (range of hues and saturation), and three intensity ranges were generated: weak, yellow; moderate, orange; strong, red; and immunonegative, blue. For pixels that satisfy the color specification, the algorithm counted the number and intensity sum in each intensity range, along with three additional quantities: average intensity, ratio of strong/total number, and average intensity of weak positive pixels. The algorithm was calibrated for both cytoplasmic and nuclear expression by constructing receiver operator curves for hue, hue width, and color saturation. A pseudocolor "markup" image was generated from the algorithm and verified to ensure that specified inputs were measuring the desired color and intensity ranges. All markup images were inspected by a pathologist (G.V.T.) to confirm the accuracy of the algorithm. The final automated score was assessed for each core as the product of corrected average intensity and corrected positive pixel percentage.

SUPPLEMENTARY MATERIAL

www.sciencetranslationalmedicine.org/cgi/content/full/3/85/85ra47/DC1

REFERENCES AND NOTES

1. K. Gupta, J. D. Miller, J. Z. Li, M. W. Russell, C. Charbonneau, Epidemiologic and socioeconomic burden of metastatic renal cell carcinoma (mRCC): A literature review. *Cancer Treat. Rev.* **34**, 193–205 (2008).
2. N. K. Janzen, H. L. Kim, R. A. Figlin, A. S. Belldegrun, Surveillance after radical or partial nephrectomy for localized renal cell carcinoma and management of recurrent disease. *Urol. Clin. North Am.* **30**, 843–852 (2003).
3. J. S. Lam, J. T. Leppert, R. A. Figlin, A. S. Belldegrun, Surveillance following radical or partial nephrectomy for renal cell carcinoma. *Curr. Urol. Rep.* **6**, 7–18 (2005).

4. S. M. Bonsib, Renal cystic diseases and renal neoplasms: A mini-review. *Clin. J. Am. Soc. Nephrol.* **4**, 1998–2007 (2009).
5. G. L. Dalgliesh, K. Furge, C. Greenman, L. Chen, G. Bignell, A. Butler, H. Davies, S. Edkins, C. Hardy, C. Latimer, J. Teague, J. Andrews, S. Barthorpe, D. Beare, G. Buck, P. J. Campbell, S. Forbes, M. Jia, D. Jones, H. Knott, C. Y. Kok, K. W. Lau, C. Leroy, M. L. Lin, D. J. McBride, M. Maddison, S. Maguire, K. McLay, A. Menzies, T. Mironenko, L. Mulderrig, L. Mudie, S. O'Meara, E. Pleasance, A. Rajasingham, R. Shepherd, R. Smith, L. Stebbings, P. Stephens, G. Tang, P. S. Tarpey, K. Turrell, K. J. Dykema, S. K. Khoo, D. Petillo, B. Wondergem, J. Anema, R. J. Kahnoski, B. T. Teh, M. R. Stratton, P. A. Futreal, Systematic sequencing of renal carcinoma reveals inactivation of histone modifying genes. *Nature* **463**, 360–363 (2010).
6. W. Y. Kim, W. G. Kaelin, Role of *VHL* gene mutation in human cancer. *J. Clin. Oncol.* **22**, 4991–5004 (2004).
7. G. V. Thomas, C. Tran, I. K. Mellinghoff, D. S. Welsbie, E. Chan, B. Fueger, J. Czernin, C. L. Sawyers, Hypoxia-inducible factor determines sensitivity to inhibitors of mTOR in kidney cancer. *Nat. Med.* **12**, 122–127 (2006).
8. B. I. Rini, M. B. Atkins, Resistance to targeted therapy in renal-cell carcinoma. *Lancet Oncol.* **10**, 992–1000 (2009).
9. B. I. Rini, J. A. Garcia, M. M. Cooney, P. Elson, A. Tyler, K. Beatty, J. Bokar, T. Mekhail, R. M. Bukowski, G. T. Budd, P. Triozzi, E. Borden, P. Ivy, H. X. Chen, A. Dolwati, R. Dreicer, A phase I study of sunitinib plus bevacizumab in advanced solid tumors. *Clin. Cancer Res.* **15**, 6277–6283 (2009).
10. R. J. Motzer, J. Bacik, T. Mariani, P. Russo, M. Mazumdar, V. Reuter, Treatment outcome and survival associated with metastatic renal cell carcinoma of non–clear-cell histology. *J. Clin. Oncol.* **20**, 2376–2381 (2002).
11. E. A. Ronnen, G. V. Kondagunta, N. Ishill, L. Spodek, P. Russo, V. Reuter, J. Bacik, R. J. Motzer, Treatment outcome for metastatic papillary renal cell carcinoma patients. *Cancer* **107**, 2617–2621 (2006).
12. G. D. Demetri, M. von Mehren, C. D. Blanke, A. D. Van den Abbeele, B. Eisenberg, P. J. Roberts, M. C. Heinrich, D. A. Tuveson, S. Singer, M. Janicek, J. A. Fletcher, S. G. Silverman, S. L. Silberman, R. Capdeville, B. Kiese, B. Peng, S. Dimitrijevic, B. J. Druker, C. Corless, C. D. Fletcher, H. Joensuu, Efficacy and safety of imatinib mesylate in advanced gastrointestinal stromal tumors. *N. Engl. J. Med.* **347**, 472–480 (2002).
13. B. J. Druker, C. L. Sawyers, H. Kantarjian, D. J. Resta, S. F. Reese, J. M. Ford, R. Capdeville, M. Talpaz, Activity of a specific inhibitor of the BCR-ABL tyrosine kinase in the blast crisis of chronic myeloid leukemia and acute lymphoblastic leukemia with the Philadelphia chromosome. *N. Engl. J. Med.* **344**, 1038–1042 (2001).
14. K. T. Laherty, I. Puzanov, K. B. Kim, A. Ribas, G. A. McArthur, J. A. Sosman, P. J. O'Dwyer, R. J. Lee, J. F. Grippo, K. Nolop, P. B. Chapman, Inhibition of mutated, activated BRAF in metastatic melanoma. *N. Engl. J. Med.* **363**, 809–819 (2010).
15. P. H. Huang, A. Mukasa, R. Bonavia, R. A. Flynn, Z. E. Brewer, W. K. Cavenee, F. B. Furnari, F. M. White, Quantitative analysis of EGFRvIII cellular signaling networks reveals a combinatorial therapeutic strategy for glioblastoma. *Proc. Natl. Acad. Sci. U.S.A.* **104**, 12867–12872 (2007).
16. J. M. Stommel, A. C. Kimmelman, H. Ying, R. Nabioullin, A. H. Ponugoti, R. Wiedemeyer, A. H. Stegh, J. E. Bradner, K. L. Ligon, C. Brennan, L. Chin, R. A. DePinho, Coactivation of receptor tyrosine kinases affects the response of tumor cells to targeted therapies. *Science* **318**, 287–290 (2007).
17. T. J. Yeatman, A renaissance for SRC. *Nat. Rev. Cancer* **4**, 470–480 (2004).
18. J. Pan, J. Mestas, M. D. Burdick, R. J. Phillips, G. V. Thomas, K. Reckamp, J. A. Belperio, R. M. Strieter, Stromal derived factor-1 (SDF-1/CXCL12) and CXCR4 in renal cell carcinoma metastasis. *Mol. Cancer* **5**, 56 (2006).
19. A. J. Pantuck, J. An, H. Liu, M. B. Rettig, NF-κB–dependent plasticity of the epithelial to mesenchymal transition induced by *Von Hippel-Lindau* inactivation in renal cell carcinomas. *Cancer Res.* **70**, 752–761 (2010).
20. S. Turcotte, D. A. Chan, P. D. Sutphin, M. P. Hay, W. A. Denny, A. J. Giaccia, A molecule targeting VHL-deficient renal cell carcinoma that induces autophagy. *Cancer Cell* **14**, 90–102 (2008).
21. R. Ishizawar, S. J. Parsons, c-Src and cooperating partners in human cancer. *Cancer Cell* **6**, 209–214 (2004).
22. D. L. Wheeler, M. Iida, E. F. Dunn, The role of Src in solid tumors. *Oncologist* **14**, 667–678 (2009).
23. R. Buettner, T. Mesa, A. Vultur, F. Lee, R. Jove, Inhibition of Src family kinases with dasatinib blocks migration and invasion of human melanoma cells. *Mol. Cancer Res.* **6**, 1766–1774 (2008).
24. P. M. Gwanmesia, A. Romanski, K. Schwarz, B. Bacic, M. Ruthardt, O. G. Ottmann, The effect of the dual Src/Abl kinase inhibitor AZD0530 on Philadelphia positive leukaemia cell lines. *BMC Cancer* **9**, 53 (2009).
25. R. E. Schweppe, A. A. Kerege, J. D. French, V. Sharma, R. L. Grzywa, B. R. Haugen, Inhibition of Src with AZD0530 reveals the Src-focal adhesion kinase complex as a novel therapeutic target in papillary and anaplastic thyroid cancer. *J. Clin. Endocrinol. Metab.* **94**, 2199–2203 (2009).
26. M. C. Frame, Src in cancer: Deregulation and consequences for cell behaviour. *Biochim. Biophys. Acta* **1602**, 114–130 (2002).
27. X. H. Zhang, Q. Wang, W. Gerald, C. A. Hudis, L. Norton, M. Smid, J. A. Foekens, J. Massagué, Latent bone metastasis in breast cancer tied to Src-dependent survival signals. *Cancer Cell* **16**, 67–78 (2009).
28. L. J. Lombardo, F. Y. Lee, P. Chen, D. Norris, J. C. Barrish, K. Behnia, S. Castaneda, L. A. Cornelius, J. Das, A. M. Doweyko, C. Fairchild, J. T. Hunt, I. Inigo, K. Johnston, A. Kamath, D. Kan, H. Klei, P. Marathe, S. Pang, R. Peterson, S. Pitt, G. L. Schieven, R. J. Schmidt, J. Tokarski, M. L. Wen, J. Wityak, R. M. Borzilleri, Discovery of *N*-(2-chloro-6-methyl-phenyl)-2-(6-(4-(2-hydroxyethyl)-piperazin-1-yl)-2-methylpyrimidin-4-ylamino)thiazole-5-carboxamide (BMS-354825), a dual Src/Abl kinase inhibitor with potent antitumor activity in preclinical assays. *J. Med. Chem.* **47**, 6658–6661 (2004).
29. Y. Liu, A. Bishop, L. Witucki, B. Kraybill, E. Shimizu, J. Tsien, J. Ubersax, J. Blethrow, D. O. Morgan, K. M. Shokat, Structural basis for selective inhibition of Src family kinases by PP1. *Chem. Biol.* **6**, 671–678 (1999).
30. P. A. Plé, T. P. Green, L. F. Hennequin, J. Curwen, M. Fennell, J. Allen, C. Lambert-Van Der Brempt, G. Costello, Discovery of a new class of anilinoquinazoline inhibitors with high affinity and specificity for the tyrosine kinase domain of c-Src. *J. Med. Chem.* **47**, 871–887 (2004).
31. K. Kondo, J. Klco, E. Nakamura, M. Lechpammer, W. G. Kaelin Jr., Inhibition of HIF is necessary for tumor suppression by the von Hippel-Lindau protein. *Cancer Cell* **1**, 237–246 (2002).
32. I. K. Lund, J. A. Hansen, H. S. Andersen, N. P. Møller, N. Billestrup, Mechanism of protein tyrosine phosphatase 1B-mediated inhibition of leptin signalling. *J. Mol. Endocrinol.* **34**, 339–351 (2005).
33. R. J. Boerner, D. B. Kassel, S. C. Barker, B. Ellis, P. DeLacy, W. B. Knight, Correlation of the phosphorylation states of $pp60^{c\text{-}src}$ with tyrosine kinase activity: The intramolecular pY530–SH2 complex retains significant activity if Y419 is phosphorylated. *Biochemistry* **35**, 9519–9525 (1996).
34. I. Moarefi, M. LaFevre-Bernt, F. Sicheri, M. Huse, C. H. Lee, J. Kuriyan, W. T. Miller, Activation of the Src-family tyrosine kinase Hck by SH3 domain displacement. *Nature* **385**, 650–653 (1997).
35. G. Sun, A. K. Sharma, R. J. Budde, Autophosphorylation of Src and Yes blocks their inactivation by Csk phosphorylation. *Oncogene* **17**, 1587–1595 (1998).
36. T. Matsubara, F. Ikeda, K. Hata, M. Nakanishi, M. Okada, H. Yasuda, R. Nishimura, T. Yoneda, Cbp recruitment of Csk into lipid rafts is critical to c-Src kinase activity and bone resorption in osteoclasts. *J. Bone Miner. Res.* **25**, 1068–1076 (2010).
37. L. Veracini, V. Simon, V. Richard, B. Schraven, V. Horejsi, S. Roche, C. Benistant, The Csk-binding protein PAG regulates PDGF-induced Src mitogenic signaling via GM1. *J. Cell Biol.* **182**, 603–614 (2008).
38. W. G. Kaelin Jr., Kidney cancer: Now available in a new flavor. *Cancer Cell* **14**, 423–424 (2008).
39. C. J. Richardson, Q. Gao, C. Mitsopoulous, M. Zvelebil, L. H. Pearl, F. M. Pearl, MoKCa database—mutations of kinases in cancer. *Nucleic Acids Res.* **37**, D824–D831 (2009).
40. N. Dubé, A. Cheng, M. L. Tremblay, The role of protein tyrosine phosphatase 1B in Ras signaling. *Proc. Natl. Acad. Sci. U.S.A.* **101**, 1834–1839 (2004).
41. T. M. Wright, W. K. Rathmell, Identification of Ror2 as a hypoxia-inducible factor target in von Hippel-Lindau-associated renal cell carcinoma. *J. Biol. Chem.* **285**, 12916–12924 (2010).
42. D. A. Chan, P. D. Sutphin, N. C. Denko, A. J. Giaccia, Role of prolyl hydroxylation in oncogenically stabilized hypoxia-inducible factor-1α. *J. Biol. Chem.* **277**, 40112–40117 (2002).
43. C. Gridelli, F. De Marinis, M. Di Maio, D. Cortinovis, F. Cappuzzo, T. Mok, Gefitinib as first-line treatment for patients with advanced non-small-cell lung cancer with activating epidermal growth factor receptor mutation: Implications for clinical practice and open issues. *Lung Cancer* **72**, 3–8 (2011).
44. C. Dahinden, B. Ingold, P. Wild, G. Boysen, V. D. Luu, M. Montani, G. Kristiansen, T. Sulser, P. Bühlmann, H. Moch, P. Schraml, Mining tissue microarray data to uncover combinations of biomarker expression patterns that improve intermediate staging and grading of clear cell renal cell cancer. *Clin. Cancer Res.* **16**, 88–98 (2010).
45. Cluster 3.0, http://bonsai.hgc.jp/~mdehoon/software/cluster/software.htm
46. TreeView, http://rana.lbl.gov/EisenSoftware.htm

47. **Acknowledgments:** We thank C. W. Ryan, W. Y. Kim, K. Ellwood-Yen, M. Ashcroft, S. Mittnacth, I. K. Mellinghoff, J. T. Erler, and R. Dresbeck for helpful discussions; J. G. Braun for academic support; L. Iwai, N. Martin, C. Garcia, P. Clarke, S. Eccles, and J. Dukes for technical expertise; M. C. Costello for artwork; W. Kaelin [Howard Hughes Medical Institute (HHMI)] for the HIF-1α and HIF-2α prolyl hydroxylase mutants; J. Massagué (HHMI) for the Src shRNA, chicken Src, and Src T388I mutant; M. Ohh for the 786-0 VHL-WT plasmid; M. Okada and S. Nada for the Csk plasmids; and T. Mori, S. McWeeney, and S. Mongue-Tchokote from the Biostatistics Shared Resource of the Knight Cancer Institute (National Cancer Institute P30 CA 069533). M.E.G. thanks the Royal Marsden Hospital foundation. **Funding:** K.M.A. is supported by National Research Service Award T32 GM71338 and award RMS1112 from the Radiological Society of

North America. P.W. is supported by Cancer Research UK program grant C309/A8274 and is a Cancer Research UK Life Fellow. This study was supported by NIH grants DK37274, CA151564 (G.T.), 1KL2 RR024141 01 through OCTRI and UL1 RR024140 (J.J.A.), R01CA149253-01 (D.Z.Q.), P30 CA069533 13S5 through OHSU Knight Cancer Institute and the Pacific Northwest Prostate Specialized Programs of Research Excellence (G.V.T.), Knight Cancer Institute award (G.T.), VHL Family Alliance, STOP Cancer Foundation, Experimental Cancer Medicine Center network and the Institute of Cancer Research (G.V.T.). **Author contributions:** N.S., E.V., K.S., H.G., and D.Z.Q. performed the cellular and biochemical experiments; M.G. conducted the immunohistochemical assays; P.S. and H.M. performed and analyzed the survival correlations; B.A.-L., D.B., and A.M.C. performed the statistical analysis on the tissue microarray and network interaction map; P.H. conducted the proteomics experiments; P.H., B.A.-L., and P.N. analyzed the proteomics data; K.M.A. and G.T. performed the in vitro kinase assays; L.G. and J.J.A. performed ChIP experiments; M.E.G., J.L., S.B.K., J.D.-B., and T.M.B. provided clinical samples for analysis and clinical insight; N.S., E.V., K.M.A., G.T., C.L.S., and P.W. provided critical input into the overall research direction; G.V.T. directed the research and wrote the manuscript with input from all the co-authors. **Competing interests:** J.D.-B. has a paid consulting relationship with AstraZeneca. The other authors declare that they have no competing interests.

Submitted 6 December 2010
Accepted 3 May 2011
Published 1 June 2011
10.1126/scitranslmed.3002004

Citation: N. Suwaki, E. Vanhecke, K. M. Atkins, M. Graf, K. Swabey, P. Huang, P. Schraml, H. Moch, A. M. Cassidy, D. Brewer, B. Al-Lazikani, P. Workman, J. De-Bono, S. B. Kaye, J. Larkin, M. E. Gore, C. L. Sawyers, P. Nelson, T. M. Beer, H. Geng, L. Gao, D. Z. Qian, J. J. Alumkal, G. Thomas, G. V. Thomas, A HIF-regulated VHL-PTP1B-Src signaling axis identifies a therapeutic target in renal cell carcinoma. *Sci. Transl. Med.* **3**, 85ra47 (2011).